

# Dynamic EPR Oximetry of Changes in Intracerebral Oxygen Tension During Induced Thromboembolism

Huagang Hou<sup>1</sup> · Nadeem Khan<sup>1</sup> · Sangeeta Gohain<sup>1</sup> · Clifford J. Eskey<sup>1</sup> · Karen L. Moodie<sup>2</sup> · Kirk J. Maurer<sup>2</sup> · Harold M. Swartz<sup>1</sup> · Periannan Kuppusamy<sup>1</sup>

Received: 22 February 2017 / Accepted: 12 April 2017 / Published online: 22 April 2017  
© Springer Science+Business Media New York 2017

**Abstract** Cerebral tissue oxygenation (oxygen tension,  $pO_2$ ) is a critical parameter that is closely linked to brain metabolism, function, and pathophysiology. In this work, we have used electron paramagnetic resonance oximetry with a deep-tissue multi-site oxygen-sensing probe, called implantable resonator, to monitor temporal changes in cerebral  $pO_2$  simultaneously at four sites in a rabbit model of ischemic stroke induced by embolic clot. The  $pO_2$  values in healthy brain were not significantly different among the four sites measured over a period of 4 weeks. During exposure to 15%  $O_2$  (hypoxia), a sudden and significant decrease in  $pO_2$  was observed in all four sites. On the other hand, brief exposure to breathing carbogen gas (95%  $O_2$  + 5%  $CO_2$ ) showed a significant increase in the cerebral  $pO_2$  from baseline value. During ischemic stroke, induced by embolic clot in the left brain, a significant decline in the  $pO_2$  of the left cortex (ischemic core) was observed without any change in the contralateral sites. While the  $pO_2$  in the non-infarct regions returned to baseline at 24-h post-stroke,  $pO_2$  in the infarct core was consistently lower compared to the baseline and other regions of the brain. The results demonstrated that electron paramagnetic resonance oximetry with the implantable resonator can repeatedly and simultaneously report temporal changes in cerebral  $pO_2$  at multiple sites. This oximetry approach can be used to

develop interventions to rescue hypoxic/ischemic tissue by modulating cerebral  $pO_2$  during hypoxic and stroke injury.

**Keywords** Cerebral ischemia · Hypoxia · EPR oximetry · Embolic stroke · Implantable oxygen sensor ·  $pO_2$

## Introduction

The cerebral tissue is the critical site for oxygen-dependent physiological and pathophysiological processes in the brain. Cerebral tissue oxygen tension ( $pO_2$ ) is closely linked with normal as well as pathophysiological processes, such as ischemic stroke, that are involved in brain injury and recovery. A precise knowledge of  $pO_2$  dynamics in the cerebral tissue immediately after an ischemic insult will be immensely useful for understanding the process of cerebral injury and to develop salvage therapies for stroke. Several methods are currently available for assessment of tissue  $pO_2$  but with limited temporal capability. The OxyLite and Licox techniques are invasive and require the insertion of probe into the tissue of interest for each measurement [1–9]. Similarly,  $^{19}F$ -MRI,  $^{15}O$ -PET, and electron paramagnetic resonance (EPR) imaging require the injection of probes for each measurement [10–19]. On the other hand, techniques such as BOLD MRI or MRI measurements of perfusion and diffusion use endogenous probes, but cannot provide direct measurement of tissue  $pO_2$ ; instead, they derive oxygen information from the levels of parameters that are indirectly related to tissue  $pO_2$  such as deoxyhemoglobin in the blood [20–25]. We have focused on the development of EPR oximetry using oxygen-sensing crystalline probe, such as lithium phthalocyanine (LiPc), which requires one-time implantation of it using a minimally invasive procedure, but

✉ Periannan Kuppusamy  
kuppu@dartmouth.edu

<sup>1</sup> Department of Radiology, The Geisel School of Medicine, Dartmouth College, 1 Medical Center Drive, Lebanon 03756 NH, USA

<sup>2</sup> Center for Comparative Medicine and Research, Dartmouth College, 1 Medical Center Drive, Lebanon 03756 NH, USA

rest of the method for  $pO_2$  measurement is entirely non-invasive and can be repeated as desired [26–29]. The basis of EPR oximetry is the paramagnetic nature of molecular oxygen, which affects the EPR linewidth of other paramagnetic species (oximetry probe), in its vicinity by altering their relaxation rates. The magnitude of change in the EPR linewidth is directly related to the amount of oxygen ( $pO_2$ ) that is present in the environment of the probe. The useful properties of LiPc for EPR oximetry are their stability and the strong response of their spectra to the presence of oxygen. The physicochemical properties of the LiPc crystals have been described earlier [30, 31]. EPR oximetry with paramagnetic oxygen-sensing materials has shown several advantages, especially for the repetitive and accurate measurement of localized tissue  $pO_2$ . However, these studies have also indicated the areas in which progress is needed, particularly the need for technological developments that can enable measurements in tissues at depths of greater than 10 mm. We have developed EPR oximetry using implantable oxygen sensors to repeatedly measure cerebral  $pO_2$  in the regions directly affected by ischemic stroke as well as the contralateral regions of the rat brain [32]. We have also systematically developed sensors that can be used to assess  $pO_2$  at depths greater than 10 mm from the surface [33]. In this paper, we report the application of an implantable resonator (IR) with four sensory tips to assess the dynamic changes in the regional oxygen levels at different depths (10 and 15 mm) in rabbit cerebral tissue for 4 weeks. We also have studied the effect of embolic stroke on cerebral  $pO_2$  in ischemic and peripheral areas in rabbits. These results indicate that EPR oximetry with multiple sensors can provide crucial information on the temporal changes in the rabbit cerebral  $pO_2$  during hypoxic/hyperoxic challenges and embolic stroke. We anticipate that this oximetry approach can also be used to study the effect of other pathologies, such as traumatic brain injury and intracranial hemorrhage on cerebral  $pO_2$  and develop interventions that can improve oxygen levels to minimize tissue damage.

## Materials and Methods

### Animal and Experimental Groups

The Dartmouth College Animal Care and Use Committee approved the animal protocol used in the study. Female New Zealand rabbits (Charles River Laboratory, Wilmington, MA), weighing 3–4 kg, were randomly divided into two experimental groups: (i) Hypoxic (15%  $O_2$ ) or hyperoxic (carbogen)-challenge group ( $N=6$ ); (ii) Embolic-stroke group (30%  $O_2$ ,  $N=5$ ). The animals had the oxygen sensor placed 3 and 7 days prior to baseline EPR

measurements for group (i) and group (2), respectively. The hypoxic/hyperoxic challenge for group (i) was repeated once a week for 4 weeks and animals with embolic stroke were subjected to a 24 h of ischemia and sacrificed right after last EPR measurements.

### Induction of Embolic Stroke

The procedures for the preparation and injection of blood clots to induce embolic stroke were acquired from the laboratory of Dr. William C. Culp (University of Arkansas for Medical Sciences, Little Rock, AK) [34–36] and modified accordingly. Briefly, blood clots were prepared using fresh rabbit blood, which was placed into a glass tube (1.5-mm inner diameter), incubated at 37 °C for 6 h and refrigerated at 4 °C for 3 days. The clots were expelled from the tube into a dish containing physiological saline and subsequently cut into several pieces of 4.0-mm in length with an average diameter of 0.6 mm. A single autologous clot was drawn into a syringe containing physiological saline (2 ml) and was injected into the internal carotid artery (ICA) with a steady flush over 10–15 s to induce ischemia. Extreme care was taken to ensure that no air bubbles were present in the syringe.

### Angiography and Embolization

Angiography was performed on rabbits in a recumbent position using OEC 9800 cardiac fluoroscope (GE Healthcare, Pittsburg, PA). Using sterile technique, a surgical cut down was performed on a common femoral artery and a 3-Fr vascular sheath was used to introduce an angiographic catheter. The customized 65-cm angled-tip 3-Fr catheter (Slip-Cath, modified JB1; Cook Inc., Bloomington, IN) was advanced using fluoroscopic guidance over a 0.025-in. angle-tip guide wire (Glidewire; Terumo Medical Corp., Elkton, MD) to the aortic arch. The image intensifier was then rotated from the frontal view to a lateral view. Another subtracted fluoroscopy injection identified the ICA for selection. Once engaged, the small catheter usually compromised ICA blood flow until withdrawn. Angiograms using hand injections of 1–2 ml of contrast in both projections showed the detailed anatomy of the entire Circle of Willies (COW). The selected clot was slowly injected with 0.7–2.0 ml of saline flush slowly following it down the catheter. A follow-up angiogram confirmed embolus arrival in the COW or a branch and localized the arterial occlusion. The catheter was then pulled back into the common carotid artery (CCA) and normal ICA flow resumed. The catheter and sheath were eventually removed, the femoral artery ligated and skin sutured.

## Evaluation of Stroke Volume

All rabbits were sacrificed after 24 h of embolic stroke and the brains were carefully removed and sectioned into 4-mm thick coronal sections, starting 4 mm from the frontal pole. The slices were placed in a 2% 2',3',5'-triphenyl-2H-tetrazolium chloride (TTC) solution at room temperature to stain viable brain, which demonstrates mitochondrial dehydrogenase activity [37]. The sections were photographed and the volume of the infarct was determined using ImageJ software by an investigator blinded to the groups.

## Paramagnetic Material and IRs

LiPc crystals, synthesized in our laboratory [31], were used as oxygen-sensing probe. The IRs were assembled with thin non-magnetic copper wires (0.3-mm wire gage) consisting of a coupling loop (12-mm diameter) at one end and a transmission line with sensor loops (0.4–0.5 mm inner diameter) at the other end (Fig. 1). The sensor loops were loaded with 30–50  $\mu\text{g}$  of LiPc crystals. The entire resonator was coated with a gas-permeable and biocompatible Teflon AF2400 [38]. The IRs are well tolerated by the animals (mice, rats, or rabbits) [32, 33, 39–41]. The mean area of the oximetry probe at the surface of each sensor loop was 1.3–1.6 mm<sup>2</sup>. EPR oximetry, therefore, samples a region that includes many capillary segments and provides average pO<sub>2</sub> at the site of the sensor loop [5, 26]. We have recently described the procedures for the placement of the IR and EPR oximetry in rabbits [33]. The diameter and the number of sensors, the length of the transmissions lines, and the distance between sensors can be adjusted based on the experimental requirements.

## Multi-Site EPR Oximetry with IR

**Surgical placement of the IR into the brain:** The surgical procedure for the placement of IR in the rabbit brain was used in strict accordance with the NIH Guide for the Care and Use of Laboratory Animals and approved by the Institutional Animal Care and Use Committee of Dartmouth College. The head of the anesthetized rabbit was antiseptically treated with betadine, and 70% alcohol scrubs. A small incision (2–3 cm) was made on the skin and burr holes were gently created by using 23–18 G needle on the skull at predefined co-ordinates: Anterior-posterior (AP from bregma): –2.0 mm; Medial-lateral (ML from midline): 4 and 8 mm on each hemisphere; Dorsal-ventral (DV from surface of skull): 15 and 10 mm in each hemisphere. These co-ordinates were based on the published reports of potential infarct region following ischemia and can be changed depending on the coordinates of the compromised tissue. The sensory points were slowly lowered at the

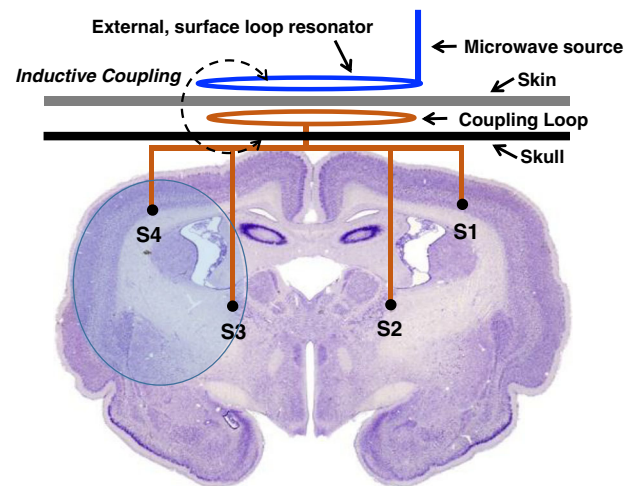


**Fig. 1** Anatomy of rabbit brain showing the location of infarct and placement of oxygen sensors. The infarct (ischemic) region is shown as shaded blue ellipse. The locations of the oxygen sensors are as follows: S4 in the cortex of ischemic core; S3 in the peripheral region; S1 in the contralateral cortex region; and S2 in the contralateral sub-cortex region. S1 and S4 were at a depth of 10 mm, while S2 and S3 were at a depth of 15 mm from the surface of skull. The coupling loop of the resonator was placed underneath the skin. An external surface loop resonator is placed above the coupling loop during pO<sub>2</sub> measurements (color figure online)

desired depth and the coupling loop was placed on the skull below the skin for inductive coupling with the external surface loop resonator of the EPR spectrometer, as shown in Fig. 1. The incision on the skin was closed with non-absorbable 3-0 nylon suture and the rabbit was monitored for recovery. Repeated measurements of cerebral pO<sub>2</sub> was started 72 h after placement of the sensors and the measurements were repeated weekly for 4 weeks.

## EPR Measurements

EPR measurements were performed using an L-band (1.2 GHz) spectrometer equipped with a surface-loop resonator and a set of gradient coils for multi-site oximetry [42, 43]. Rabbit, anesthetized using 2.5% isoflurane in 30% O<sub>2</sub>, was positioned in the EPR magnet and surface-loop resonator was placed over the head region. A magnetic field gradient of 1.7 G/cm was used to separate the EPR spectra from each sensor for simultaneous multisite oximetry [44, 45]. Analysis of the EPR spectra was performed using software written using Matlab (Mathworks, Inc., Natick, MA). The peak-to-peak line-width of the EPR spectra was used to determine pO<sub>2</sub> using a standard curve. The rabbit was maintained at 38 ± 1.0 °C (monitored via a rectal probe) by keeping the animal warm with warm air during the EPR measurements. The EPR settings were: incident microwave power: 0.4–1.2 mW; modulation frequency 24 kHz; magnetic field center 410 G; scan time 10 s, scan range 8–12 G,

and modulation amplitude not exceeding one-third of the line width.

Three-to-seven days after placement of the IR, anesthesia was administered via inhalation using 3.5% isoflurane and maintained with 2.5–3.0% of isoflurane with 30% oxygen through a sealed nose cone at a flow rate of 2.0 l/min. Baseline EPR measurements were made in all rabbits for a period of 30 min to measure the pO<sub>2</sub>. During EPR measurements, the animal temperature was maintained using a thermostatically-controlled heated pad and warm air forced through the core of the magnet. The heart rate and blood oxygen saturation were continuously measured using a pulse oximeter (Nonin 8600 V Pulse Oximeter, Phoenix, Arizona) throughout the EPR measurements.

#### Hypoxic/Hyperoxic Challenge

The rabbits were anesthetized with 2–3.0% isoflurane in 30% oxygen through a nose cone and a baseline pO<sub>2</sub> was measured for 25 min using EPR oximetry as described above. After the baseline pO<sub>2</sub> measurements, animals were subjected sequentially to mild hypoxia (15% O<sub>2</sub> for 18 min), normoxia (30% O<sub>2</sub> for 20 min), normobaric hyperoxia (carbogen for 20 min) and normoxia (30% O<sub>2</sub> for 15 min).

#### Embolic clot stroke

Seven days after placement of the sensor, the animals were anesthetized (2.5–3.0% isoflurane with 30% oxygen) and a pre-treatment (baseline) pO<sub>2</sub> measurements was made for 30 min at the four sites. Thereafter, embolic clot stroke was induced and pO<sub>2</sub> measurements were repeated for 50 min,

during which all the animals continued to breathe 30% oxygen. At 24 h of post-embolic-clot stroke, pO<sub>2</sub> measurements were repeated for 60 min during which all the animals continued to breathe 30% oxygen.

#### Statistical Analysis

A paired *t*-test was used to compare the pO<sub>2</sub> values at four sites and during baseline, hypoxia/hyperoxia challenges and embolic clot stroke within the same group. The paired comparison reduces the effects of animal-to-animal heterogeneity and eliminates differences in the baseline pO<sub>2</sub>. The tests were two-sided and a change with a *p*-value <0.05 was considered statistically significant. All data are expressed as mean ± SEM.

### Results and Discussion

#### Cerebral pO<sub>2</sub> Dynamics During Hypoxic and Hyperoxic Interventions

We tested the capability of EPR oximetry for temporal monitoring of cerebral pO<sub>2</sub> under normal and altered oxygen-inhalation conditions. Cerebral pO<sub>2</sub> was continuously measured while the breathing gas was cycled through 30% O<sub>2</sub> (normoxia), 15% O<sub>2</sub> (to simulate hypoxia during cerebral ischemia), and 95% O<sub>2</sub> (hyperoxia). We used 30% O<sub>2</sub> inhalation instead of room air (~21% O<sub>2</sub>) breathing to maintain normoxic pO<sub>2</sub> level by compensating for the loss of tissue oxygenation under isoflurane anesthesia. Figure 2 shows the cerebral pO<sub>2</sub> values measured

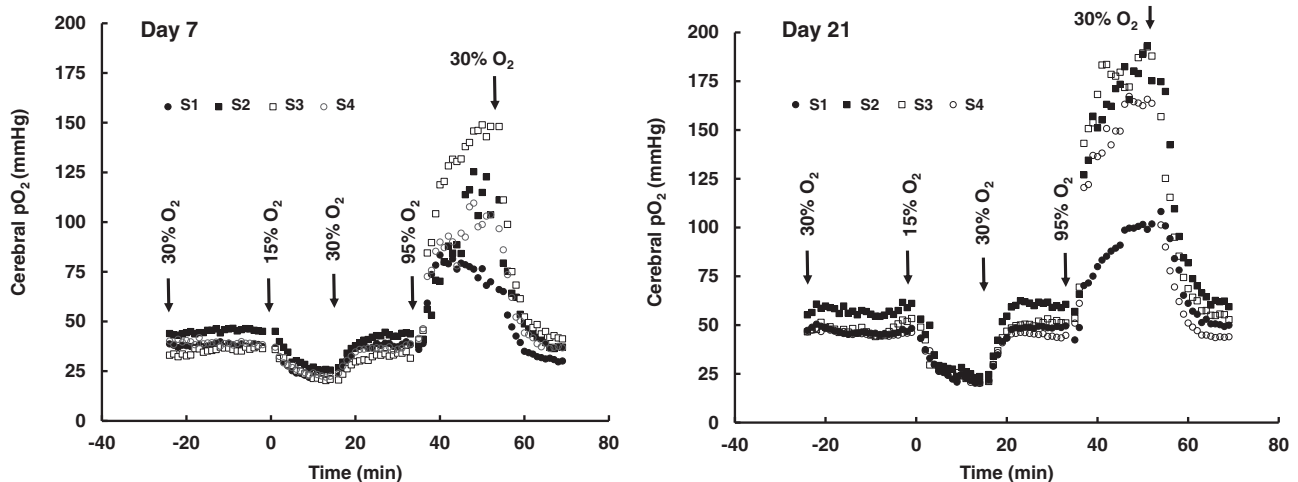


**Fig. 2** Changes in cerebral pO<sub>2</sub> measured in a rabbit subjected to hypoxic and hyperoxic breathing. An IR with four sensory tips (S1–S4) was implanted at two sites in each hemisphere, as shown in Fig. 1. pO<sub>2</sub> measurements were made on the same rabbit on day 7 and

day 21 after sensor placement. Oxygen content in the inhalation gas was varied as indicated. The results show a consistent variation of pO<sub>2</sub> among all four sites up on exposure to different oxygen levels

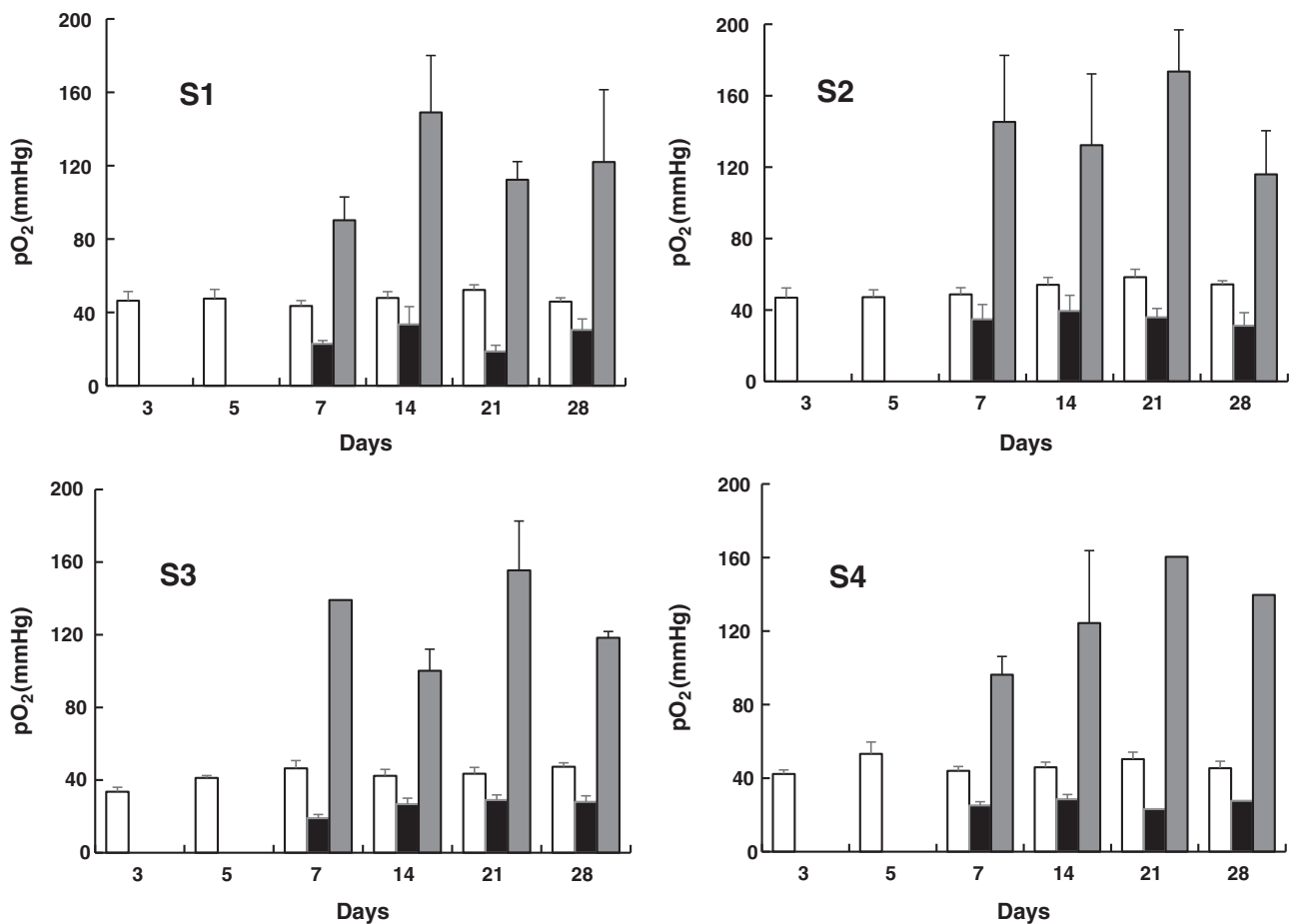


**Fig. 3** Cerebral pO<sub>2</sub> measured over a 4-week period. The pO<sub>2</sub> measurements were performed simultaneously at four sites (S1–S4) using EPR oximetry under conditions of breathing normal (□ 30% O<sub>2</sub>), low

(■ 15% O<sub>2</sub>) and high (■ 95% O<sub>2</sub>) oxygen. Data represent mean ± SEM obtained from five rabbits

from a rabbit on day 7 and repeated on day 21 at multiple locations as shown in Fig. 1. The results showed a quick decline in cerebral pO<sub>2</sub> at all four sites when the composition of the breathing gas was switched from 30 to 15% O<sub>2</sub>. A sharp increase in the cerebral pO<sub>2</sub> was observed when the breathing gas was switched from 30 to 95% O<sub>2</sub> (carbogen gas). The responses to hypoxia and hyperoxia were similar among the four sites; however, the magnitudes of change during hyperoxia were significantly different. An exponential quadratic function of time analyses indicated that it took 10–14 min to reach equilibrium after hypoxic or hyperoxic challenge (data not shown). It should be noted that similar responses were observed on both days suggesting that neither the tissue nor integrity of the sensors was changed during the two-week period.

To determine the reliability of the multi-site sensor for long-term monitoring of tissue pO<sub>2</sub>, measurements were repeated on a group of rabbits for four consecutive weeks following the sensor placement. Figure 3 shows the average pO<sub>2</sub> values at each of the four sites obtained from a total of

five rabbits during a 4-week period. The data showed, in general, a 40% decline during hypoxic (15% O<sub>2</sub>) intervention and a 60% surge during hyperoxic (95% O<sub>2</sub>) intervention. The mean baseline pO<sub>2</sub> data obtained from each of the four sites over the 4-week period were in the range 34–57 mmHg (Fig. 4). The pO<sub>2</sub> averaged over all sites and animals showed a consistent variation up on hypoxia or hyperoxia intervention suggesting that, in general, there were no substantial variations in the cerebral pO<sub>2</sub> among the sites in the normal brain. We also observed a similar increase in cerebral tissue pO<sub>2</sub> in mice and rats breathing carbogen [39, 46–48]. Overall, the results established the capability of EPR oximetry to obtain reliable measurements repeatedly and simultaneously from multiple sites in the brain.

### Cerebral pO<sub>2</sub> During Embolic-Clot Stroke

We used a minimally invasive angiographic approach to induce embolic-clot stroke in rabbits [34, 49–52]. This

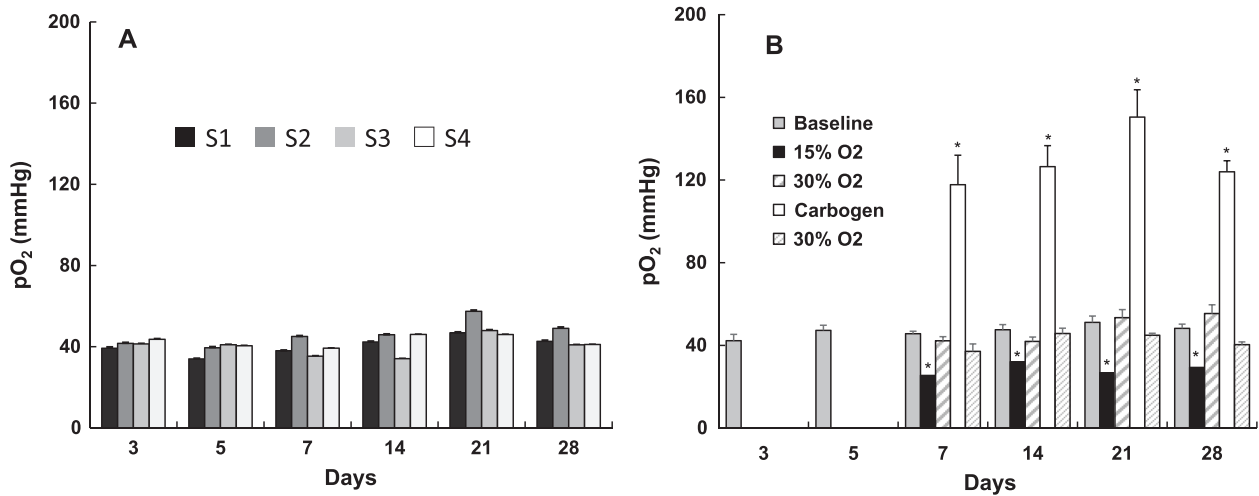


**Fig. 4** Cerebral pO<sub>2</sub> and its response to oxygen breathing. **a** Mean pO<sub>2</sub> values obtained from the four sites (S1–S4) while the rabbits ( $N = 5$ ) were breathing 30% O<sub>2</sub>. **b** Mean pO<sub>2</sub> from the four sites during baseline (30% O<sub>2</sub>), inhalation of 15% O<sub>2</sub>, recovery from 15% O<sub>2</sub>

breathing, inhalation of 95% O<sub>2</sub> (carbogen) and recovery. Data represent mean  $\pm$  SEM,  $N = 5$ . \* $p < 0.01$  compared to baseline pO<sub>2</sub> on each day (paired  $t$ -test)

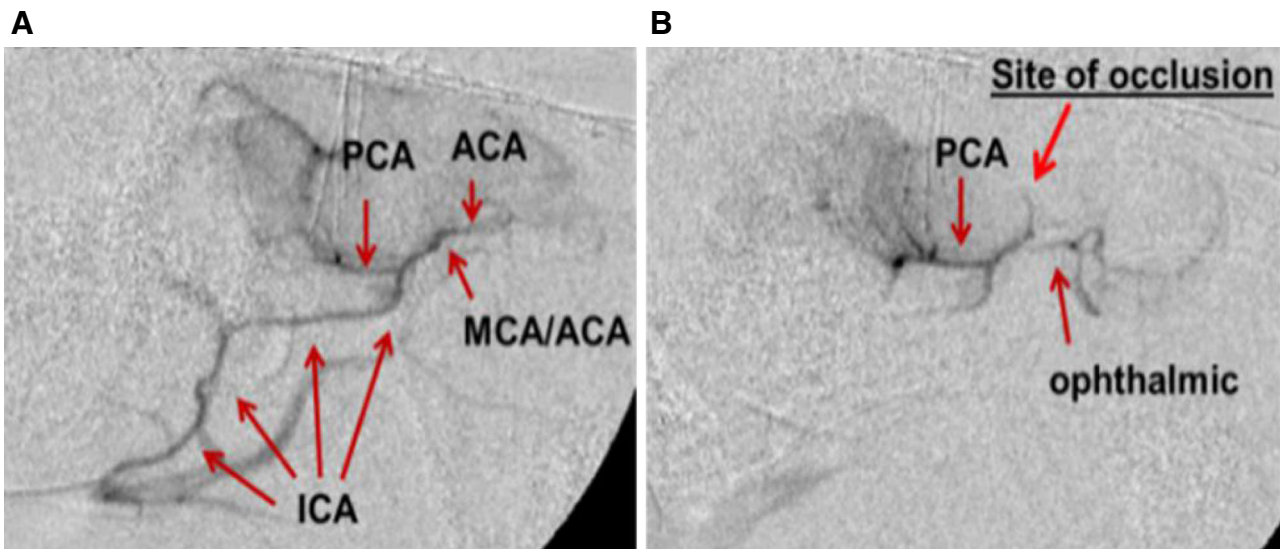


**Fig. 5** Angiographic images showing arterial occlusion following ischemic stroke. Arterial network in **a** pre-stroke and **b** post-stroke induced by embolic blood clot as described in the Methods section.

*ICA* internal carotid artery, *MCA* middle cerebral artery, *ACA* anterior cerebral artery, *PCA* posterior cerebral artery

approach involves transarterial injection of pre-formed blood clot to model human cerebral thromboembolism. The angiographic access to the ICA is obtained via cannulation of the femoral artery in the hind limb of the rabbits. This approach is less invasive than other approaches that involve major surgery in the neck and/or brain region to induce stroke [53, 54]. The angiographic approach also avoids surgical distortions in the regional arteries supplying the brain, does not occlude the CCA thereby preserving inflow, and provides a pure embolic defect. The injection of large pre-aged clots (4-mm length, 3 days) not only mimics

major stroke, but can also be lysed by tissue plasminogen activator. This model simulates the human embolic stroke in which occlusive material, usually clot or atheroma, is dislodged and passed into the large cerebral arteries. This model also allows one to immediately confirm the presence and location of the occlusion (Fig. 5) [55].

To perform EPR oximetry in the emboli-stroke model a, we first determined the typical locations of infarct core and penumbra in five test rabbits, which were not part the study groups. Using this information, we could target the resonator implantation so that the sensors could be in each of the

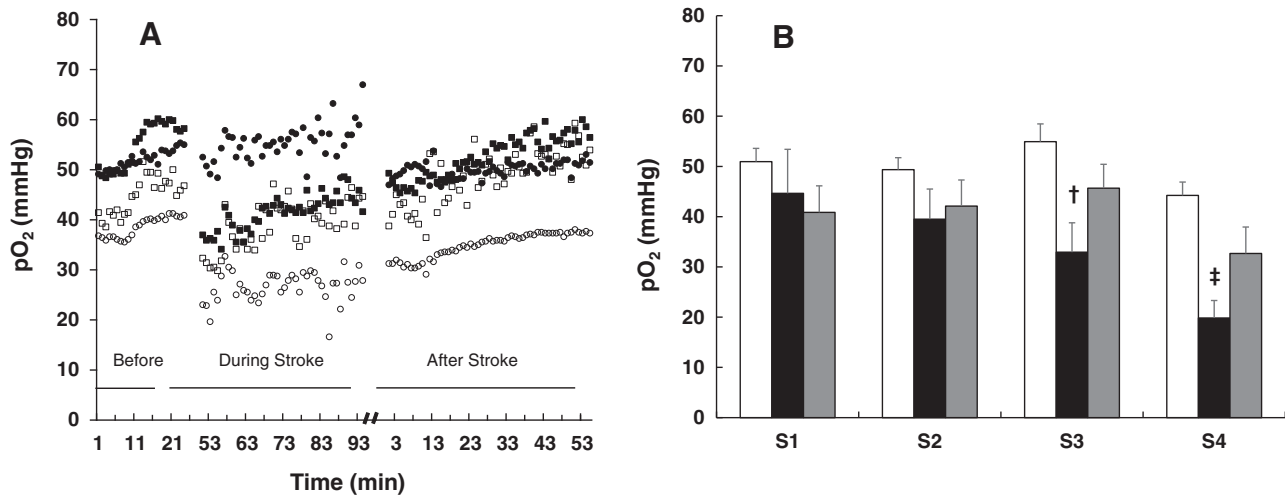


**Fig. 6** Cerebral pO<sub>2</sub> at four different sites in the rabbit brain with stroke. **a** Changes in pO<sub>2</sub> in the ischemic core (S4; ○), contralateral cortex (S1; ●), peripheral region (S3, □) and contralateral sub-cortex (S2, ■) before, during and after induction of stroke. **b** Mean pO<sub>2</sub> levels

at each site during baseline, at 30-min post-stroke and at 24-h post-stroke. Data represent mean ± SEM ( $N = 3-5$ ). <sup>†</sup> $p < 0.05$ ; <sup>‡</sup> $p < 0.01$ , compared with baseline pO<sub>2</sub> (paired  $t$ -test)

following locations: infarct core (S4), ischemic penumbra (S3) and matching regions in the other cerebral hemisphere (S2, S1). After acquiring pO<sub>2</sub> measurements in rabbits breathing 30% O<sub>2</sub> (baseline), clot was injected to induce ischemic stroke. Cerebral pO<sub>2</sub> was monitored immediately after the occlusion and 24 h later (Fig. 6). A significant and rapid decline in the pO<sub>2</sub> of the infarct core and ischemic penumbra was evident (Fig. 6). No change in the pO<sub>2</sub> of the contralateral region was observed. Tissue pO<sub>2</sub> in the penumbra (S3) returned to baseline at 24-h post-stroke; however, low levels of pO<sub>2</sub> in the infarct core persisted during this period. The results demonstrated the capability of EPR oximetry for real-time monitoring of ischemia induction and oxygen dynamics during the development of embolic clot-induced stroke. Such direct and repeated measurements of oxygen levels in the brain will provide valuable insight on the temporal changes during ischemic stroke and will facilitate evaluation of the hyperoxic strategies to improve oxygen levels and treatment outcome.

### Measurement of Physiology and Infarct Volume

The arterial oxyhemoglobin saturation, heart rate, and core temperature of animals breathing 30% O<sub>2</sub> were stable. SpO<sub>2</sub> values significantly decreased during hypoxia (15% O<sub>2</sub>) as compared to the baseline. On the other hand, a significant increase in arterial oxyhemoglobin saturation after carbogen inhalation was observed when compared to the baseline (data not shown). The arterial oxyhemoglobin saturation, heart rate, and core temperature of animals at 30 min and 24 h after embolic clot stroke were stable (data not shown). Figure 7 shows the axial view of whole rabbit brain with the

track of the implantable sensor on the surface and infarction in rostral and caudal coronal sections of the brain after 24 h of embolization. A close examination of the tissue sections revealed that the sensors S4 and S3 were in the infarct core and ischemic penumbra regions, respectively, in all five rabbits. Quantitation of the infarct volume indicated a significant infarct in the ischemic hemisphere of all surviving rabbits in embolic clot stroke group.

The results presented in this report is part of our systematic study to characterize the changes in brain pO<sub>2</sub> during inhalation of hypoxic and hyperoxic gases using in vivo EPR oximetry. We have previously reported the effect of breathing hypoxic (10–15% O<sub>2</sub>) and hyperoxic (100% O<sub>2</sub>, carbogen and hyperbaric oxygen therapy) challenges on the brain pO<sub>2</sub> in rats and rabbits with the goal to understand the sensitivity of IRs to local changes of brain pO<sub>2</sub> and how improved oxygen levels protect brain from ischemic stroke in the brain [28, 29, 32, 33].

### Conclusions

The results of the present study demonstrated the capability of EPR oximetry to perform repeated measurements of cerebral pO<sub>2</sub> simultaneously at multiple sites. The method enables reliable measurements of temporal changes in cerebral pO<sub>2</sub> under pathophysiological conditions over a period of weeks. The dynamic information of cerebral pO<sub>2</sub> can be used to test and to optimize strategies for improving treatment outcome of ischemic stroke.

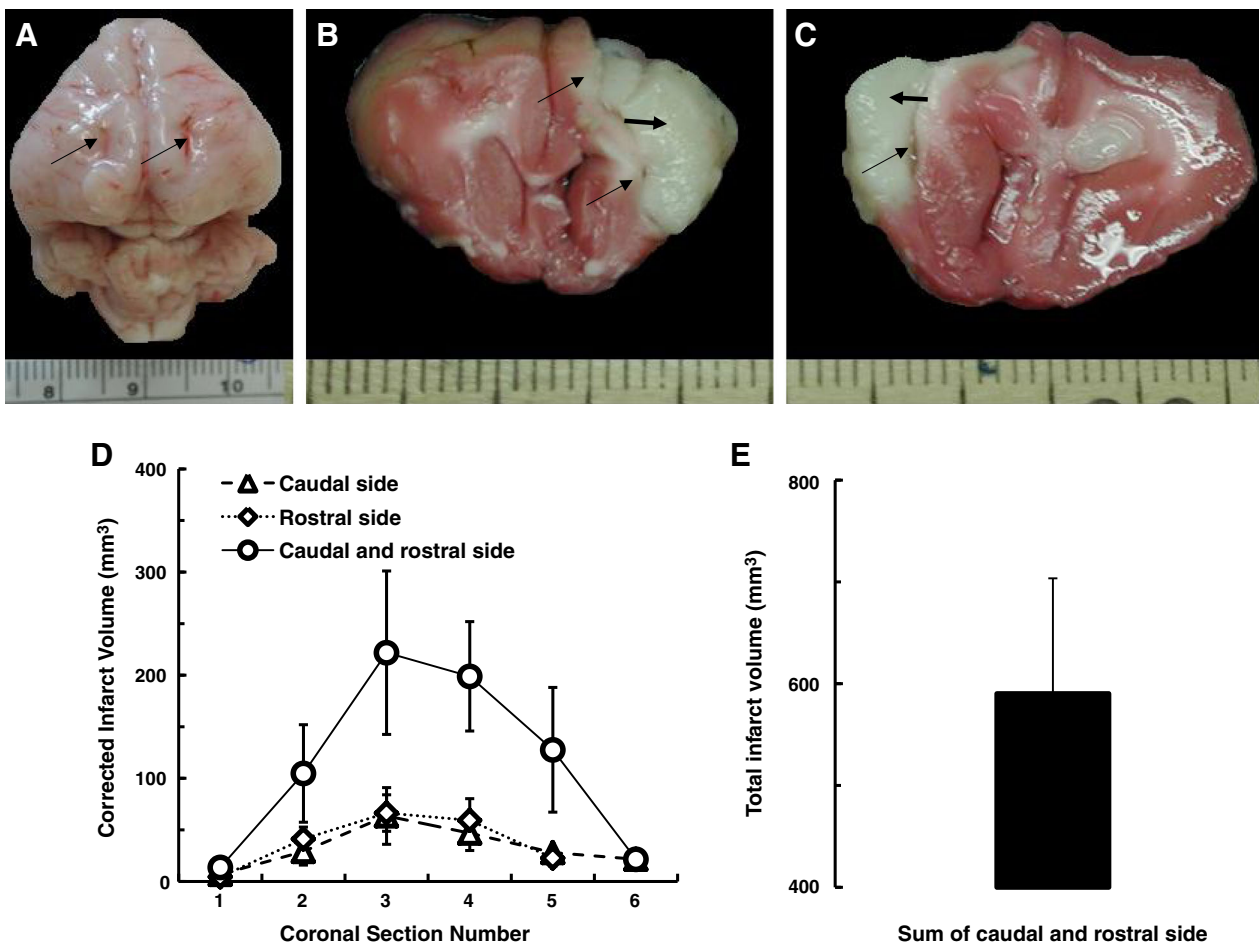


**Fig 7** Coronal sections and infarct size. **a** Axial view of whole rabbit brain with the track of the implantable sensor on the surface indicated by *long arrows*. **b** Rostral and **c** caudal coronal sections of the brain after 24 h of arterial embolization showing the infarct region indicated by *short arrow*. **d** Infarct volume in each of the six coronal sections for rostral and caudal sides. **e** Total infarct volume summed over the six sections for rostral and caudal sides. Corrected infarct area = measured infarct area  $\times$  area of contralateral corresponding structure/area of

ipsilateral corresponding structure. Infarction volumes for continuous macrosections =  $\Sigma(\text{thickness} \times \frac{1}{2} (\text{corrected infarct area of a section's rostral surface} + \text{corrected infarct area of a section's caudal surface}))$ . The thickness of each section is 5 mm and was stained with the vital dye TTC. Viable areas stain *red* and non-viable areas remain white indicated with *black short arrow*. The *scale bars* represent the millimeters

**Acknowledgements** This work was supported by National Institutes of Health grants NS082585 and EB004031.

#### Compliance with Ethical Standards

**Conflict of Interest** The authors declare that they have no competing interest.

#### References

- Griffiths, J. R., & Robinson, S. P. (1999). The OxyLite: A fibre-optic oxygen sensor. *British Journal of Radiology*, 72(859), 627–630.
- Braun, R. D., Lanzen, J. L., Snyder, S. A., & Dewhirst, M. W. (2001). Comparison of tumor and normal tissue oxygen tension measurements using OxyLite or microelectrodes in rodents. *American Journal of Physiology-Heart and Circulatory Physiology*, 280(6), H2533–H2544.
- Seddon, B. M., Honess, D. J., Vojnovic, B., Tozer, G. M., & Workman, P. (2001). Measurement of tumor oxygenation: In vivo comparison of a luminescence fiber-optic sensor and a polarographic electrode in the p22 tumor. *Radiation Research*, 155(6), 837–846.
- Urano, M., Chen, Y., Humm, J., Koutcher, J. A., Zanzonico, P., & Ling, C. (2002). Measurements of tumor tissue oxygen tension using a time-resolved luminescence-based optical OxyLite probe: Comparison with a paired survival assay. *Radiation Research*, 158(2), 167–173.
- O'Hara, J. A., Hou, H., Demidenko, E., Springett, R. J., Khan, N., & Swartz, H. M. (2005). Simultaneous measurement of rat brain cortex PtO<sub>2</sub> using EPR oximetry and a fluorescence fiber-optic sensor during normoxia and hyperoxia. *Physiological Measurement*, 26(3), 203–213.
- Vikram, D. S., Bratasz, A., Ahmad, R., & Kuppusamy, P. (2007). A comparative evaluation of EPR and OxyLite oximetry using a



- random sampling of pO(2) in a murine tumor. *Radiation Research*, 168(3), 308–315.
7. Dengl, M., Jaeger, M., Renner, C., & Meixensberger, J. (2012). Comparing brain tissue oxygen measurements and derived autoregulation parameters from different probes (Licox vs. Raumedic). *Acta Neurochirurgica*, 114, 165–168.
  8. Keddie, S., & Rohman, L. (2012). Reviewing the reliability, effectiveness and applications of Licox in traumatic brain injury. *Nursing in Critical Care*, 17(4), 204–212.
  9. Morgalla, M. H., Haas, R., Grozinger, G., Thiel, C., Thiel, K., Schuhmann, M. U., & Schenk, M. (2012). Experimental comparison of the measurement accuracy of the Licox(R) and Raumedic (R) Neurovent-PTO brain tissue oxygen monitors. *Acta Neurochirurgica*, 114, 169–172.
  10. Tran, L. B., Bol, A., Labar, D., Jordan, B., Magat, J., Mignon, L., Gregoire, V., & Gallez, B. (2012). Hypoxia imaging with the nitroimidazole 18F-FAZA PET tracer: A comparison with Oxy-Lite, EPR oximetry and 19F-MRI relaxometry. *Radiotherapy and Oncology*, 105(1), 29–35.
  11. Orringer, D. A., Vago, D. R., & Golby, A. J. (2012). Clinical applications and future directions of functional MRI. *Seminars in Neurology*, 32(4), 466–475.
  12. Krishna, M. C., Matsumoto, S., Yasui, H., Saito, K., Devashayam, N., Subramanian, S., & Mitchell, J. B. (2012). Electron paramagnetic resonance imaging of tumor pO(2). *Radiation Research*, 177(4), 376–386.
  13. Horsman, M. R., Mortensen, L. S., Petersen, J. B., Busk, M., & Overgaard, J. (2012). Imaging hypoxia to improve radiotherapy outcome. *Nature Reviews Clinical Oncology*, 9(12), 674–687.
  14. Giraudeau, C., Djemai, B., Ghaly, M. A., Boumezbeur, F., Meriaux, S., Robert, P., Port, M., Robic, C., Le Bihan, D., Lethimonnier, F., & Valette, J. (2012). High sensitivity 19F MRI of a perfluorooctyl bromide emulsion: Application to a dynamic biodistribution study and oxygen tension mapping in the mouse liver and spleen. *NMR in Biomedicine*, 25(4), 654–660.
  15. Gaertner, F. C., Souvatzoglou, M., Brix, G., & Beer, A. J. (2012). Imaging of hypoxia using PET and MRI. *Current Pharmaceutical Biotechnology*, 13(4), 552–570.
  16. Liu, S., Shah, S. J., Wilmes, L. J., Feiner, J., Kodibagkar, V. D., Wendland, M. F., Mason, R. P., Hylton, N., Hopf, H. W., & Rollins, M. D. (2011). Quantitative tissue oxygen measurement in multiple organs using 19F MRI in a rat model. *Magnetic Resonance in Medicine*, 66(6), 1722–1730.
  17. Baete, S. H., Vandecasteele, J., & De Deene, Y. (2011). 19F MRI oximetry: Simulation of perfluorocarbon distribution impact. *Physics in Medicine and Biology*, 56(8), 2535–2557.
  18. Ahmad, R., Caia, G., Potter, L. C., Petyakov, S., Kuppusamy, P., & Zweier, J. L. (2010). In vivo multisite oximetry using EPR-NMR coimaging. *Journal of Magnetic Resonance*, 2207(1), 69–77.
  19. Runge, V.M. (2013). Current technological advances in magnetic resonance with critical impact for clinical diagnosis and therapy. *Investigative Radiology*, 48(12), 869–877.
  20. Christen, T., Bolar, D. S., & Zaharchuk, G. (2013). Imaging brain oxygenation with MRI using blood oxygenation approaches: Methods, validation, and clinical applications. *American journal of neuroradiology*, 34(6), 1113–1123.
  21. Blockley, N. P., Griffith, V. E., Simon, A. B., & Buxton, R. B. (2013). A review of calibrated blood oxygenation level-dependent (BOLD) methods for the measurement of task-induced changes in brain oxygen metabolism. *NMR in Biomedicine*, 26(8), 987–1003.
  22. Vikram, D. S., Zweier, J. L., & Kuppusamy, P. (2007). Methods for noninvasive imaging of tissue hypoxia. *Antioxidants & Redox Signaling*, 9(10), 1745–1756.
  23. Tuunanen, P. I., & Kauppinen, R. A. (2006). Effects of oxygen saturation on BOLD and arterial spin labelling perfusion fMRI signals studied in a motor activation task. *Neuroimage*, 30(1), 102–109.
  24. Dunn, J. F., O'Hara, J., Zaim-Wadghiri, Y., Zhu, H., Lei, H., Meyerand, M. E., Grinberg, O., Hou, H. G., Hoopes, P. J., Demidenko, E., & Swartz, H. M. (2002). Changes in oxygenation of intracranial tumors with carbogen, an MR "BOLD" imaging and EPR oximetry study. *Journal of Magnetic Resonance Imaging*, 16, 511–521.
  25. Demeure, R. J., Jordan, B. F., Yang, Q. X., Beghein, N., Smith, M. B., Gregoire, V., & Gallez, B. (2002). Removal of local field gradient artefacts in BOLD contrast imaging of head and neck tumours. *Physics in Medicine and Biology*, 10, 1819–1825.
  26. Khan, N., Williams, B. B., Hou, H., Li, H., & Swartz, H. M. (2007). Repetitive tissue pO2 measurements by electron paramagnetic resonance oximetry: Current status and future potential for experimental and clinical studies. *Antioxidants & Redox Signaling*, 9(8), 1169–1182.
  27. Hou, H., Khan, N., O'Hara, J. A., Grinberg, O. Y., Dunn, J. F., Abajian, M. A., Wilmot, C. M., Demidenko, E., Lu, S., Steffen, R. P., & Swartz, H. M. (2005). Increased oxygenation of intracranial tumors by efaproxyn (efaproxiral), an allosteric hemoglobin modifier: In vivo EPR oximetry study. *International Journal of Radiation Oncology, Biology, Physics*, 61(5), 1503–1509.
  28. Hou, H., Grinberg, O. Y., Grinberg, S. A., Demidenko, E., & Swartz, H. M. (2005). Cerebral tissue oxygenation in reversible focal ischemia in rats: Multi-site EPR oximetry measurements. *Physiological Measurement*, 26(1), 131–141.
  29. Hou, H., Grinberg, O., Williams, B., Grinberg, S., Yu, H., Alvarenga, D. L., Wallach, H., Buckley, J., & Swartz, H. M. (2007). The effect of oxygen therapy on brain damage and cerebral pO(2) in transient focal cerebral ischemia in the rat. *Physiological Measurement*, 28(8), 963–976.
  30. Swartz, H. M., & Clarkson, R. B. (1998). The measurement of oxygen in vivo using EPR techniques. *Physics in Medicine and Biology*, 43(7), 1957–1975.
  31. Liu, K. J., Gast, P., Moussavi, M., Norby, S. W., Vahidi, N., Walczak, T., Wu, M., & Swartz, H. M. (1993). Lithium phthalocyanine: A probe for electron paramagnetic resonance oximetry in viable biological systems. *Proceedings of the National Academy of Sciences of the United States of America*, 90(12), 5438–5442.
  32. Hou, H., Li, H., Dong, R., Khan, N., & Swartz, H. (2014). Real-time monitoring of ischemic and contralateral brain pO2 during stroke by variable length multisite resonators. *Magnetic Resonance Imaging*, 32(5), 563–569.
  33. Khan, N., Hou, H., Eskey, C. J., Moodie, K., Gohain, S., Du, G., Hodge, S., Culp, W. C., Kuppusamy, P., & Swartz, H. M. (2015). Deep-tissue oxygen monitoring in the brain of rabbits for stroke research. *Stroke*, 46(3), e62–e66.
  34. Culp, W. C., Woods, S. D., Brown, A. T., Lowery, J. D., Hennings, L. J., Skinner, R. D., Borrelli, M. J., & Roberson, P. K. (2013). Three variations in rabbit angiographic stroke models. *Journal of Neuroscience Methods*, 212(2), 322–328.
  35. Woods, S. D., Flores, R., Roberson, P. K., Lowery, J. D., Skinner, R. D., & Culp, W. C. (2011). Decreased serum levels of S-100B protein reflect successful treatment effects in a rabbit model of acute ischemic stroke. *Open Neurology Journal*, 5, 55–57.
  36. Hennings, L. J., Flores, R., Roberson, P. K., Brown, A., Lowery, J., Borrelli, M., & Culp, W. C. (2011). Persistent penumbra in a rabbit stroke model: Incidence and histologic characteristics. *Stroke Research and Treatment*, 2011, 764830.
  37. Bederson, J., Pitts, L., Germano, S., Nishimura, M., Davis, R., & Bartkowski, H. (1986). Evaluation of 2,3,5-triphenyltetrazolium

- chloride as a stain for detection and quantification of experimental cerebral infarction in rats. *Stroke*, 17(6), 1304–1308.
38. Dinguzli, M., Jeumont, S., Beghein, N., He, J., Walczak, T., Lesniewski, P. N., Hou, H., Grinberg, O. Y., Sucheta, A., Swartz, H. M., & Gallez, B. (2006). Development and evaluation of biocompatible films of polytetrafluoroethylene polymers holding lithium phthalocyanine crystals for their use in EPR oximetry. *Biosensors & Bioelectronics*, 21(7), 1015–1022.
  39. Hou, H., Dong, R., Li, H., Williams, B., Lariviere, J. P., Hekmatyar, S. K., Kauppinen, R. A., Khan, N., & Swartz, H. (2012). Dynamic changes in oxygenation of intracranial tumor and contralateral brain during tumor growth and carbogen breathing: A multisite EPR oximetry with implantable resonators. *Journal of Magnetic Resonance*, 214(1), 22–28.
  40. Hou, H., Li, H., Dong, R., Mupparaju, S., Khan, N., & Swartz, H. (2011). Cerebral oxygenation of the cortex and striatum following normobaric hyperoxia and mild hypoxia in rats by EPR oximetry using multi-probe implantable resonators. *Advances in Experimental Medicine and Biology*, 701, 61–67.
  41. Li, H., Hou, H., Sucheta, A., Williams, B. B., Lariviere, J. P., Khan, M. N., Lesniewski, P. N., Gallez, B., & Swartz, H. M. (2010). Implantable resonators—a technique for repeated measurement of oxygen at multiple deep sites with in vivo EPR. *Advances in Experimental Medicine and Biology*, 662, 265–272.
  42. Hirata, H., Walczak, T., & Swartz, H. M. (2000). Electronically tunable surface-coil-type resonator for L-band EPR spectroscopy. *Journal of magnetic Resonance*, 142(1), 159–167.
  43. Salikhov, I., Hirata, H., Walczak, T., & Swartz, H. M. (2003). An improved external loop resonator for in vivo L-band EPR spectroscopy. *Journal of Magnetic Resonance*, 164(1), 54–59.
  44. Smirnov, A. I., Norby, S. W., Clarkson, R. B., Walczak, T., & Swartz, H. M. (1993). Simultaneous multi-site EPR spectroscopy in vivo. *Magnetic Resonance in Medicine*, 30(2), 213–220.
  45. Hou, H., Mupparaju, S. P., Lariviere, J. P., Hodge, S., Gui, J., Swartz, H. M., & Khan, N. (2013). Assessment of the changes in 9L and C6 glioma pO<sub>2</sub> by EPR oximetry as a prognostic indicator of differential response to radiotherapy. *Radiation Research*, 179(3), 343–351.
  46. Hou, H., Dong, R., Lariviere, J. P., Mupparaju, S. P., Swartz, H. M., & Khan, N. (2011). Synergistic combination of hyperoxygenation and radiotherapy by repeated assessments of tumor pO<sub>2</sub> with EPR oximetry. *Journal of Radiation Research*, 52(5), 568–574.
  47. Khan, N., Mupparaju, S., Hekmatyar, S. K., Hou, H., Lariviere, J. P., Demidenko, E., Gladstone, D. J., Kauppinen, R. A., & Swartz, H. M. (2010). Effect of hyperoxygenation on tissue pO<sub>2</sub> and its effect on radiotherapeutic efficacy of orthotopic F98 gliomas. *International Journal of Radiation Oncology, Biology, Physics*, 78(4), 1193–1200.
  48. Khan, N., Li, H., Hou, H., Lariviere, J. P., Gladstone, D. J., Demidenko, E., & Swartz, H. M. (2009). Tissue pO<sub>2</sub> of orthotopic 9L and C6 gliomas and tumor-specific response to radiotherapy and hyperoxygenation. *International Journal of Radiation Oncology, Biology, Physics*, 73(3), 878–885.
  49. Brown, A., Woods, S., Skinner, R., Hatton, J., Lowery, J., Roberson, P., Hennings, L., & Culp, W. C. (2013). Neurological assessment scores in rabbit embolic stroke models. *Open Neurology Journal*, 7, 38–43.
  50. Brown, A. T., Skinner, R. D., Flores, R., Hennings, L., Borrelli, M. J., Lowery, J., & Culp, W. C. (2010). Stroke location and brain function in an embolic rabbit stroke model. *Journal of Vascular and Interventional Radiology*, 21(6), 903–909.
  51. Culp, B. C., & Culp, W. C. (2008). Rabbit subselective angiography stroke model. *Stroke*, 39(11), e165 author reply e166.
  52. Culp, B. C., Brown, A. T., Erdem, E., Lowery, J., & Culp, W. C. (2007). Selective intracranial magnification angiography of the rabbit: Basic techniques and anatomy. *Journal of Vascular and Interventional Radiology*, 18(2), 187–192.
  53. Chen, Z. Z., Jiang, X. D., Zhang, L. L., Shang, J. H., Du, M. X., Xu, G., & Xu, R. X. (2008). Beneficial effect of autologous transplantation of bone marrow stromal cells and endothelial progenitor cells on cerebral ischemia in rabbits. *Neuroscience Letters*, 445(1), 36–41.
  54. Lapchak, P. A. (2010). Translational stroke research using a rabbit embolic stroke model: A correlative analysis hypothesis for novel therapy development. *Translational Stroke Research*, 1(2), 96–107.
  55. Li, H., Hou, H., Sucheta, A., Williams, B. B., Lariviere, J. P., Khan, M. N., Lesniewski, P. N., Gallez, B., & Swartz, H. M. (2010). Implantable resonators—a technique for repeated measurement of oxygen at multiple deep sites with in vivo EPR. *Advances in Experimental Medicine and Biology*, 662, 265–272.